RSC Advances

This is an *Accepted Manuscript*, which has been through the Royal Society of Chemistry peer review process and has been accepted for publication.

Accepted Manuscripts are published online shortly after acceptance, before technical editing, formatting and proof reading. Using this free service, authors can make their results available to the community, in citable form, before we publish the edited article. This *Accepted Manuscript* will be replaced by the edited, formatted and paginated article as soon as this is available.

You can find more information about *Accepted Manuscripts* in the Information for Authors.

Please note that technical editing may introduce minor changes to the text and/or graphics, which may alter content. The journal's standard Terms & Conditions and the Ethical guidelines still apply. In no event shall the Royal Society of Chemistry be held responsible for any errors or omissions in this *Accepted Manuscript* or any consequences arising from the use of any information it contains.

ROYAL SOCIETY OF CHEMISTRY

www.rsc.org/advances

Adsorption and corrosion inhibition properties of N-{*n*-[1-*R*-5-(quinoxalin-6-yl)-4,5-dihydropyrazol-3-yl]phenyl}methanesulfonamides on mild steel in 1 M HCl: Experimental and theoretical studies

Lukman O. Olasunkanmi,[a,b,c] Ime B. Obot,[d] Eno E. Ebenso[a,b*]

[a]*Department of Chemistry, School of Mathematics and Physical Sciences, Faculty of Agriculture, Science and Technology, North-West University (Mafikeng Campus) Private Bag X2046, Mmabatho 2735, South Africa.*
[b]*Material Science Innovation and Modelling (MaSIM) Research Focus Area, Faculty of Agriculture, Science and Technology, North-West University (Mafikeng Campus) Private Bag X2046, Mmabatho 2735, South Africa.*
[c]*Department of Chemistry, Faculty of Science, ObafemiAwolowo University, Ile-Ife, 220005, Nigeria.*
[d]*Centre of Research Excellence in Corrosion, Research Institute, King Fahd University of Petroleum and Minerals, Dhahran 31261, Kingdom of Saudi Arabia*

**Corresponding Author; E-mail: Eno.Ebenso@nwu.ac.za; Tel: +27 183892050/2051; Fax: +27183892052*

Abstract

Six quinoxalinyl-dihydropyrazolyl-phenyl-methanesulfonamides were investigated for their adsorption characteristics and inhibition of mild steel corrosion in 1 M HCl medium. Tafel polarization measurements revealed that all the studied compounds are mixed-type inhibitors. Electrochemical impedance spectroscopy showed that the compounds form pseudo-capacitive protective film on mild steel surface and protect the steel from direct acid attack. The inhibitors adsorb on mild steel in 1 M HCl via competitive physisorption and chemisorption mechanisms and their adsorption obeyed the Langmuir adsorption isotherm model. UV-vis spectra confirmed that the inhibitors interact with mild steel in solution to form Fe-inhibitor complexes. Scanning electron microscope (SEM) images also confirmed the protective efficacy of the studied compounds on mild steel in the acid. Quantum chemical calculations and quantitative structure activity relationship (QSAR) studies proposed good correlations between molecular quantum chemical descriptors and experimental inhibition efficiencies. Descriptors for protonated species correlate better than those of neutral species. Adsorption of the studied molecules was simulated on Fe(110) surface and the binding energies derived from molecular dynamics simulations corroborate experimental results. Compounds in which sulfonamido group is attached to position 3 on the phenyl ring showed higher corrosion inhibition activities.

RSC Advances Accepted Manuscript

1 Introduction

Corrosion of metals is still considered a foremost source of economic and safety concerns to industries. This is in spite of copious research progress that has been documented in corrosion science and technology.[1] Corrosion tends to occur in almost all aqueous environments,[2] but the process is grievously shaped up in more aggressive media such as those encountered in oil and gas industries. Oil and gas processing and allied activities such as pipeline cleaning, pipeline/acid descaling and oil-well acidizing involve the use of mineral acids, most especially hydrochloric and sulphuric acids.[3] Acid washing, matrix acidizing, and fracture acidizing involve pumping of acid (usually hydrochloric acid) into the well with the aim of improving well productivity or injectivity.[4,5] These unavoidable production activities unfortunately expose the metal alloys that made up the oil well and pipelines to acid corrosion.

An ample number of studies in corrosion science researches focus on mild steel corrosion and prevention.[6-15] The popularity of mild steel in this regards is connected with its wild usage, owing to its relatively high mechanical strength and low cost.[6-10] As a type of carbon steel, mild steel also has advantages of ease of fabrication, availability, and weldability over many other metal alloys.[16,17] However, mild steel is highly susceptible to corrosion in common aqueous environments, especially acidic solutions.[18,19] A comparative analysis of cost and efficiencies of known corrosion control and prevention methods puts the use of corrosion inhibitors at a rational edge.[1] Apart from the fact that many corrosion inhibitors can be synthesized from relatively cheap materials,[1] their utilization proffers a convenient approach of repressing metal corrosion.[20] Inhibitors can be injected into production channels in situ without necessarily disrupting the on-going production process.[20,21] Many applications involve the use of corrosion inhibitors in conjunction with other methods such as coating and cathodic protection to achieve more enhanced protection efficiency.[1]

Oxidizing inhibitors such as chromates and nitrates were popular in the earlier stage of corrosion inhibition studies. The major drawbacks in using these materials include the poisonous nature of chromates. In addition, the use of these compounds below some critical concentrations can favour localized corrosion and the resulting effects may be worse than no inhibitor at all.[22] Organic compounds that contain π electron systems and heteroatoms such as N, O, S and P have been reported to exhibit good protection efficiencies. In a review on promising novel corrosion inhibitors, Gece[23] reported the advantages of using drugs, chemical medicines or biologically active compounds as corrosion inhibitors. The central

RSC Advances Accepted Manuscript

benefit of using drug-like compounds as corrosion inhibitors is their fairly non-toxicity and less detrimental effects on the environment.[23]

Many drugs and biologically important compounds contain quinoxalines[24-29] and sulphonamides[29-33] as essential units or fragments. These compounds have been reported to exhibit a wide spectrum of biological activities, including antitumor, antiepileptic, antibiotics, and anticancer activities.[24-35] The inhibitive effects of quinoxaline[9,36-46] and sulphonamide[47-50] derivatives on metal corrosion have also been established. The inhibition potentials of organic compounds mainly depend on their ability to adsorb on metallic surface and form protective film. The modes of adsorption and corrosion inhibition potentials are influenced by many factors, which include the electronic structure, steric hindrance, π-electron network, and electron density at donor/acceptor sites of the inhibitor. For this reason, investigations of the mode of adsorption and corrosion inhibition properties of new organic compounds that are promising corrosion inhibitors appear to be a continuous and dynamic area of research.

In the present study, six quinoxalinyl-dihydropyrazolyl-phenyl-methanesulfonamides namely, N-(2-(1-propanoyl-5-(quinoxalin-6-yl)-4,5-dihydro-1H-pyrazol-3-yl)phenyl)methanesulfonamide (MS-2-PQPP), N-(3-(1-propanoyl-5-(quinoxalin-6-yl)-4,5-dihydro-1H-pyrazol-3-yl)phenyl)methanesulfonamide (MS-3-PQPP), N-(4-(1-propanoyl-5-(quinoxalin-6-yl)-4,5-dihydropyrazol-3-yl)phenyl)methanesulfonamide (MS-4-PQPP), N-(2-(1-(methanesulfonyl)-5-(quinoxalin-6-yl)-4,5-dihydro-1H-pyrazol-3-yl)phenyl)methanesulfonamide(MS-2-PQPMS), N-{3-[1-(methylsulfonyl)-5-(quinoxalin-6-yl)-4,5-dihydro-1H-pyrazol-3-yl]phenyl}methanesulfonamide (MS-3-PQPMS), and N-(4-(1-(methanelsulfonyl)-5-(quinoxalin-6-yl)-4,5-dihydro-1H-pyrazol-3-yl)phenyl)methanesulfonamide (MS-4-PQPMS) were investigated for their adsorption and corrosion inhibition properties on mild steel in 1 M HCl solution. The selection of these compounds as potential corrosion inhibitors in this study is premised on their drug-likeness, low toxicity,[23] and the presence of moieties (quinoxaline and sulphonamide) with proven metal protection abilities.[36-50] The quinoxaline derivatives were divided into two groups (MS-*n*-PQPP and MS-*n*-PQPMS groups (n = 2,3,4)) based on some levels of similarity and specific variation in their molecular structure and substituent functional groups. Experimental electrochemical studies were carried out using Tafel polarization and electrochemical impedance spectroscopy (EIS) techniques. Ultraviolet-visible (UV-vis) spectroscopic technique was used to substantiate metal-inhibitor interactions. Scanning electron microscopic images of the surfaces of mild steel specimens immersed in the (non)inhibitior-containing acid solutions were taken and reported. Theoretical quantum chemical calculations

RSC Advances Accepted Manuscript

and molecular dynamic simulation studies were carried out on the studied molecules to corroborate experimental results.

It is important to mention that the compounds studied in this work are being considered as corrosion inhibitors for the first time. More so, works that employ the kind of detailed theoretical studies presented in the present work to support experimentations are scanty. To the best of our knowledge this is also the first time proton affinity (PA) of organic compounds is being proven as a weighty quantum chemical descriptor in the formulation of quantitative structure activity relationship (QSAR) empirical equations for corrosion inhibitors.

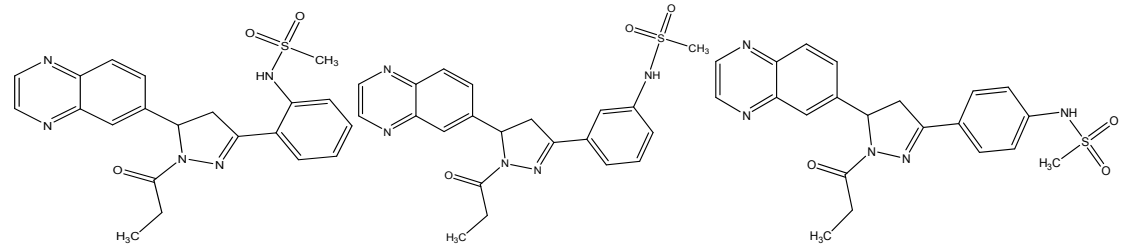

MS-2-PQPP MS-3-PQPP MS-4-PQPP

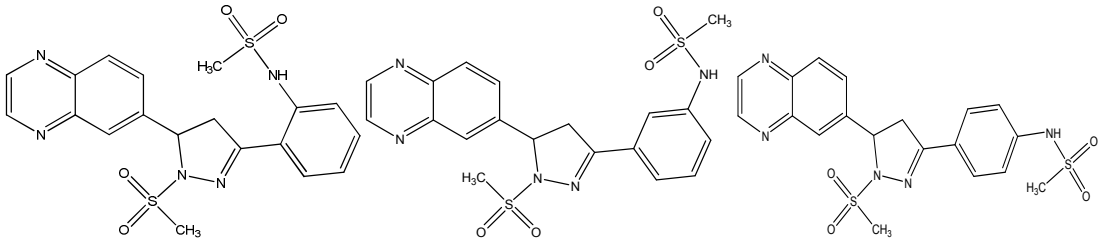

MS-2-PQPMS MS-3-PQPMS MS-4-PQPMS

Fig. 1. 2D molecular structures of the studied compounds.

2 Experimental details

2.1 Mild steel specimens

The elemental compositions (in weight per cent) of the mild steel sheets used for the corrosion tests are Carbon (0.17 %), Manganese (0.46 %), Silicon (0.26 %), Sulphur (0.017 %), Phosphorus (0.019 %), and balance Fe. For the purpose of electrochemical studies, mild steel sheets were cut into 1 cm × 1 cm dimension, glued to a connecting wire using aluminium foil tape, and embedded in a silico-rubber mould with the aid of epoxy resin. The fabricated mild steel utilized as the working electrode (WE) has an exposed area of 1 cm^2, necessary to ensure uniform contact area for electrochemical reactions.

The surface of the mild steel WE was mechanically abraded on Struers MD Piano 220 (size: 200 dia) mounted on Struers LaboPol-1 machine to remove traces of epoxy resin from

RSC Advances Accepted Manuscript

the surface. Mild steel surface was ground with SiC paper of graded grit sizes ranging from 600 to 1200 to obtain a polished surface free of pre-experimental corrosion products. The surface was then washed with water, degreased in acetone, washed with distilled water again, before finally dried with clean white towel paper. All electrochemical experiments were carried out using freshly surface pre-treated mild steel WE.

2.2 Aggressive electrolyte solutions

Hydrochloric acid of 32 % assay was commercially obtained from Promark chemicals, South Africa, and diluted with distilled water to prepare the 1 M HCl solution (pH = 0) used for the experiments. The quinoxaline derivatives were obtained from Vitas-M Laboratory, Ltd., Apeldoorn the Netherlands; Life Chemicals Inc., Munich, Germany; Enamine Ltd., New Jersey, United States of America, and ChemBridge Corporation, San Diego, United States of America and used without further purifications. Concentrations of the inhibitor solutions used for the experiments range from 5 ppm to 100 ppm.

2.3 Electrochemical measurements

All electrochemical measurements were carried out on the Autolab PGSTAT 302N equipped with a three-electrode electrochemical cell system comprising Ag/AgCl in 3 M KCl as the reference electrode (RE), platinum rod as the counter electrode (CE), and mild steel WE. The Autolab PGSTAT 302N equipment was driven by the Nova 1.10.1.9 software. The adopted steps for the electrochemical set-up and measurements have been successfully utilized in previous works.[7,17,45,51-54] A period of 30 minutes was allowed for the electrochemical system to reach the steady open circuit potential (OCP) or corrosion potential (E_{corr}) after immersion of the WE before each electrochemical perturbations. This period considered sufficient for OCP stabilization for an electrochemical system consisting of mild steel in acidic medium.[45,52-62]

Tafel polarization curves were obtained by sweeping the potential up to ±100 mV[63,64] with respect to the E_{corr} at the scan rate of 1 mV/s.[64-67] The EIS measurements were conducted at the E_{corr} by passing AC-signals through the electrochemical system and analyzing the frequency response between 100 kHz and 100 mHz at 5 mV peak-to-peak amplitude.[53] All electrochemical experiments were conducted under aerated unstirred conditions at 303 K.

Corrosion inhibition efficiency ($\%IE_p$) was calculated from the Tafel polarization measurements as:[45,55,59,60,68-71]

RSC Advances Accepted Manuscript

$$\%IE_P = 100\left(\frac{i^0_{corr} - i_{corr}}{i^0_{corr}}\right) \quad (1)$$

where i^0_{corr} and i_{corr} are corrosion current densities without and with various concentrations of inhibitors respectively. Corrosion inhibition efficiency ($\%IE_I$) was estimated from the EIS measurements using the equation:[45,55,56,59,60,68-71]

$$\%IE_I = 100\left(\frac{R_{ct} - R^0_{ct}}{R_{ct}}\right) \quad (2)$$

where R_{corr} and R^0_{corr} are the charge transfer resistances with and without various concentrations of inhibitors respectively. The surface coverage (θ) is related to the percentage inhibition efficiency ($\%IE$) as:[72]

$$\theta = \frac{\%IE}{100} \quad (3)$$

2.4 UV-vis spectroscopic studies

The UV-vis spectroscopic technique is often used in corrosion inhibition studies to inform the formation inhibitor-metal complex.[54,55,73,74] In order to confirm possible formation of inhibitor-Fe complexes, UV–vis absorption spectra of 1 M HCl solutions containing 100 ppm of each quinoxaline derivative were recorded before and after 3 h of mild steel immersion.

2.5 Surface morphology studies

Mild steel specimens with freshly pre-treated surface were immersed in 1 M HCl solutions without and with 100 ppm of the studied compounds. The specimens were retrieved after 3 h and the surfaces were examined using the quanta FEG 250 environmental scanning electron microscope (ESEM) equipment obtained from IMP Scientific & Precision (PTY) Ltd. Boksburg, Gauteng, South Africa.

2.6 Quantum chemical calculations

Geometry optimizations and vibrational frequency calculations were carried out on the neutral and singly protonated forms of the studied quinoxaline derivatives. Geometry optimizations were performed without symmetry constraint using the density functional theory (DFT) method. Hybrid functional, B3LYP comprising the Becke's three parameter exchange functional[75] and Lee-Yang-Parr correlation functional[76,77] was used in conjunction with 6-31G(d) basis set for all the calculations. The B3LYP functional has been widely used in literature in conjunction with different Pople's basis sets to produce satisfactory geometries

RSC Advances Accepted Manuscript

at relatively less computational cost.[78-81] All the possible sites of protonation were considered for the singly protonated species in order to identify the most favourable site of protonation. The reason for considering the protonated species is premised on the possibility of these compounds to undergo protonation in acidic medium such that the protonated species could take part in the corrosion inhibition process. Optimized structures were confirmed to correspond to true energy minima conformers by the absence of imaginary vibrational frequency. All the calculations were carried out in the gas phase with the aid of Gaussian 09W (revised version D.01) software.[82]

The frontier molecular orbital (FMO) energy parameters including energy of the highest occupied molecular orbital (E_{HOMO}) and energy of the lowest unoccupied molecular orbital (E_{LUMO}) were obtained for both the neutral and protonated forms of the inhibitor molecules. Other relevant parameters such absolute hardness, η and absolute electronegativity, χ were calculated using the respective equations:[83,84]

$$\eta = \frac{1}{2}(E_{LUMO} - E_{HOMO}) \quad (4)$$

$$\chi = -\frac{1}{2}(E_{HOMO} + E_{LUMO}) \quad (5)$$

The fraction of electrons transferred (ΔN) from the inhibitor (donating) molecule to the metallic (Fe) atom (acceptor) was calculated according to the equation:[85]

$$\Delta N = \frac{\chi_{Fe} - \chi_{inh}}{2(\eta_{Fe} + \eta_{inh})} \quad (6)$$

where χ_{Fe} and η_{inh} denote the electronegativity and hardness of iron and inhibitor respectively. A value of 7 eV/mol was used for the χ_{Fe}, while η_{Fe} was equated to 0 eV/mol for bulk Fe atom in line with the Pearson's electronegativity scale.[86]

2.7 Molecular dynamics (MD) simulations

Molecular dynamic (MD) simulations were carried out to model the adsorption behaviour of the studied inhibitors on iron (Fe) surface. The simulations were used to compute the binding or interaction energies of the lowest configuration interactions between the inhibitors molecules and clean iron surface. The simulations were carried out by using the forcite module in the Material Studio software 7.0 from BIOVIA-Accelrys, USA. The Fe was cleaved along (110) plane and a slab of 5 Å was employed. The Fe(110) surface was used for the simulations because it provides adequate representation of the Fe surface with sufficient stability and moderate atom density.[41,87,88] The Fe(110) plane has been successfully applied in

RSC Advances Accepted Manuscript

the literature to describe the interactions between inhibitor molecules and Fe surface.[41,45,87-94] The Fe (110) plane was enlarged to a (10 × 10) super cell to provide a large surface for the interaction of the inhibitors. A vacuum slab with 30 Å thickness was built above the Fe (110) plane. The simulations were performed in NVT canonical ensemble at 298K with a time step of 1.0 fs and a total simulation time of 500 ps using Anderson thermostat.

The condensed-phase optimized molecular potentials for atomistic simulation studies (COMPASS) force field was used to optimize the structures of all components of the system of interest. The COMPASS force field is an ab initio force field that enables accurate and simultaneous predictions of gas-phase properties (structural, conformational, vibrational, etc.) and condensed-phase (equation of state, cohesive energies, interaction energies, etc.) for a broad range of organic molecules, inorganic molecules and metals.[95-99]

The interaction energy (E_{int}) of molecules with Fe surface was obtained using the equation:

$$E_{int} = E_{total} - (E_{surface} + E_{molecule}) \quad (7)$$

Where E_{total} is the total energy of the molecules and the metal surface system; $E_{surface}$ is the energy of metal surface without adsorption of molecules, and $E_{molecule}$ is the energy of the isolated inhibitor molecule. The binding energy ($E_{binding}$) is the negative of the interaction energy (i.e. $E_{binding} = -E_{int}$).

3 Results and discussion

3.1 Electrochemical studies

3.1.1 Tafel plots

Tafel polarization curves were obtained for mild steel in 1 M HCl without and with various concentrations of the studied inhibitors and the results are presented in Fig. 2 for MS-2-PQPP and MS-2-PQPMS. Similar curves were obtained for the other compounds (Fig. S1). For all the six compounds tested as inhibitors, the curves shift towards lower current density region in the presence of the inhibitors compared to the blank acid medium. This suggests that the studied compounds reduce the corrosion current and therefore reduce the corrosion rate. The polarization curves also exhibit some shifts in potential towards more anodic or cathodic regions relative to the acid blank. The direction of the shift is not uniform as it varies with concentrations of the inhibitors. This suggests that the inhibitors affect both the anodic and cathodic corrosion reactions.

Kinetic parameters for the corrosion reactions in the absence and presence of different concentrations of the inhibitors were obtained from the Tafel plots by extrapolating the linear Tafel regions to the corrosion potential. The results obtained via Tafel extrapolations are

RSC Advances Accepted Manuscript

listed in Table 1. The observed shift in E_{corr} of the inhibitor containing system relative to the blank is generally less than 85 mV for all the studied compounds. This suggests that the studied compounds might be mixed-type inhibitors.[55,65,100-102] In other words, the compounds inhibit both the anodic (mild steel dissolution) reaction and the cathodic reactions. The cathodic reactions in this case may include hydrogen gas evolution (i.e. $2H^+ + 2e^- \rightarrow H_2O$) and oxygen reduction (i.e. $4H^+ + O_2 + 4e- \rightarrow 2H_2O$), since the experiment was conducted in aerated acidic solution. However, the oxygen reduction may not be prominent under the prevailing experimental conditions because it has been reported that the effect of dissolved oxygen on iron corrosion in acid is only more significant at pH greater than 4.[103] Besides, the variation in the E_{corr} seems negligible with the maximum shift of about ± 17 mV. This observation suggests that the addition of the studied inhibitors does not (or only weakly) perturb the mild steel electrode surface.[104] Such a small shift in the E_{corr} has also been attributed to the geometric blocking of the active sites on the steel surface by the inhibitor molecules.[105,106]

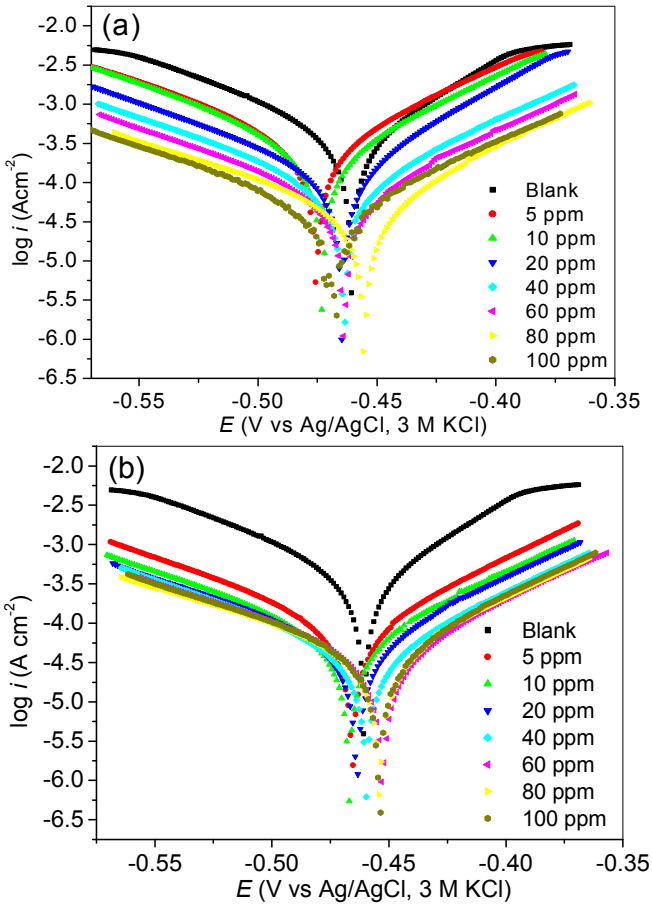

Fig. 2. Tafel plots for mild steel in 1 M HCl without and with various concentrations of (a) MS-2-PQPP, and (b) MS-2-PQPMS, as representative Tafel plots for the studied compounds.

RSC Advances Accepted Manuscript

Table 1. Tafel parameters and percentage inhibition efficiency for the corrosion of MS in 1 M HCl without and with inhibitors.

Compound	*Conc.* (ppm)	- E_{corr} (mV)	i_{corr}(μA/cm^2)	β_a (mV/dec)	β_c (mV/dec)	$\%IE_P$
Blank	-	460.60	420.41	89.34	65.27	-
MS-2-PQPP	5	475.46	318.55	93.84	77.90	24.19
	10	473.01	251.66	88.54	75.81	40.11
	20	464.90	137.89	96.81	59.76	67.20
	40	463.73	95.73	101.36	76.51	77.22
	60	463.72	70.20	102.01	76.58	83.29
	80	468.43	50.11	105.91	81.71	88.08
	100	455.35	51.34	116.70	71.85	87.78
MS-3-PQPP	5	463.98	142.63	97.59	73.44	66.06
	10	457.67	62.37	97.00	67.40	85.16
	20	461.61	54.87	91.42	74.03	86.94
	40	456.72	55.71	111.01	71.14	86.74
	60	446.76	40.69	112.77	70.54	90.32
	80	445.78	42.57	126.68	70.87	89.87
	100	440.36	41.35	137.58	68.03	90.16
MS-4-PQPP	5	465.03	148.12	130.50	95.46	64.75
	10	463.62	120.81	114.64	84.47	71.25
	20	462.93	98.12	121.64	83.28	76.65
	40	457.26	70.76	110.17	71.31	83.16
	60	457.30	50.36	99.82	67.95	88.02
	80	436.70	46.39	130.28	71.25	88.96
	100	446.57	41.50	122.28	68.82	90.12
MS-2-PQPMS	5	465.56	89.66	94.52	73.95	78.66
	10	467.08	64.91	96.26	74.48	84.55
	20	461.70	59.02	106.98	76.13	85.96
	40	459.43	42.86	98.11	75.83	89.80
	60	452.64	42.62	111.11	74.89	89.86
	80	453.96	45.89	120.66	77.68	89.08
	100	453.77	45.36	114.33	74.23	89.20
MS-3-PQPMS	5	460.43	69.86	97.47	70.14	83.38
	10	455.11	55.91	96.89	62.17	86.70
	20	451.55	62.18	111.60	74.69	86.23
	40	463.79	61.68	115.64	95.61	85.32
	60	443.09	42.83	115.71	67.38	89.81
	80	459.91	48.15	111.61	91.19	88.54
	100	454.09	41.20	109.76	84.44	90.20
MS-4-PQPMS	5	456.99	131.53	96.36	71.75	68.70
	10	458.81	70.27	104.07	67.77	83.28
	20	454.72	69.87	109.05	71.62	83.37
	40	455.70	44.17	104.41	75.84	89.49
	60	447.36	45.38	115.74	70.34	89.20
	80	454.99	45.19	110.94	73.80	89.25
	100	450.79	38.47	115.60	72.06	90.84

RSC Advances Accepted Manuscript

The values of the Tafel slopes, β_a and β_c vary slightly with concentrations of the inhibitors, but without a simple definite pattern. However, the values of β_a and β_c in the presence of the inhibitors are generally higher than those of the blank. The variation in the values of the Tafels slopes with change in the concentration of the inhibitors also seems more apparent for β_a than β_c. These observations suggest the formation of some inhibitor complexes of Fe in the low and higher oxidation states on the mild steel electrode surface.[9,107] This is suggestive of more inhibitive actions of the compounds on the anodic reaction than the cathodic one.

The corrosion current density, i_{corr} decreases with increase in concentration of the inhibitors leading to increase in inhibition efficiency ($\%IE_P$). The $\%IE_P$ of MS-2-PQPP increases from 24.19 % at 5 ppm up to 88.08 % at 80 ppm. Further increase in concentration does not show any significant effect on inhibition efficiency. The trend of the inhibition performance of MS-3-PQPP is such that there is an apparent increase in inhibition efficiency as the concentration of the inhibitor increases from 5 ppm to 10 ppm. The values of the $\%IE_P$ at 20 ppm and 40 ppm are nearly the same. A maximum value of 90.32 % was obtained at 60 ppm after which further increase in concentration does not seem to have noticeable effect on protection efficiency. The $\%IE_P$ of MS-4-PQPP increases continuously as the concentration increases from 5 ppm to 100 ppm. Similar trends were obtained for MS-2-PQPMS, MS-3-PQPMS and MS-4-PQPMS.

The increase in inhibition efficiency with increasing concentration may be attributed to increase in the number of adsorbed molecules of the inhibitor on the steel surface. The number of molecules that adsorb on the active sites on the steel surface increase with increasing concentration of the inhibitor, leading to an increase in surface coverage, and consequently, increase in inhibition efficiency. It is difficult to establish a simple trend for the protection efficiencies of the compounds but the overall performance based on the average values of $\%IE_P$ within the concentration range considered in this work is MS-3-PQPP > MS-4-PQPP > MS-2-PQPP; and MS-3-PQPMS > MS-2-PQPMS > MS-4-PQPMS.

3.1.2 EIS measurements

Nyquist and Bode plots were obtained for mild steel in 1 M HCl in the absence and presence of various concentrations of the studied inhibitors. The representative plots are shown in Fig. 3 for MS-2-PQPP. Similar profiles were obtained for other compounds (Figs. S2 and S3). The EIS spectra show similar behaviour in the absence and presence of the inhibitors, which suggests that the inhibition of steel corrosion in the acid by the studied compounds does not alter the mechanism of the corrosion process.[3,52,108]

RSC Advances Accepted Manuscript

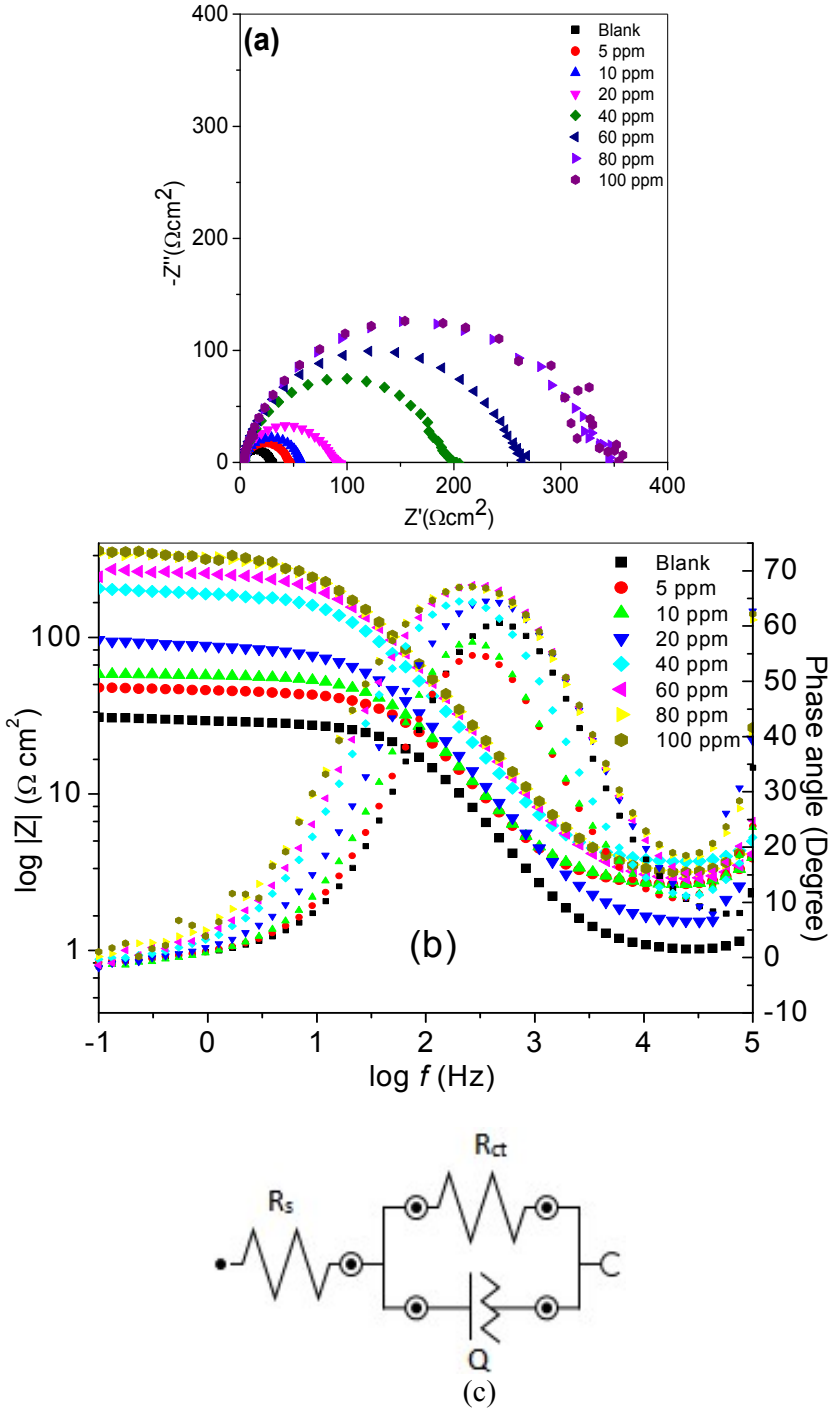

Fig. 3. Nyquist (a) and Bode (b) plots for mild steel in 1 M HCl without and with various concentrations of MS-2-PQPP as the representative impedance spectra of the studied compounds; (c) equivalent circuit for the EIS spectra.

The Nyquist plots show single depressed semicircles corresponding to one time-constant in the Bode plots. The depression of a Nyquist semicircle is attributed to frequency dispersion effects that may result from roughness of the electrode surface and/or other forms

RSC Advances Accepted Manuscript

of interfacial phenomena.[109,110] The depressed one time-constant semicircular Nyquist profiles show capacitive behaviour at low frequencies, which suggests that the corrosion of mild steel in the studied media is controlled by charge transfer process. The diameters of the Nyquist semicircles in the presence of the inhibitors are generally larger than that of the uninhibited system. This implies the mild steel/electrolyte systems exhibit higher impedance to flow of charges in the presence of the inhibitors. This is indicative of the inhibitive effect of the studied compounds.

The EIS spectra were fitted to the equivalent circuit model of the form in Fig. 3c. The values of electrochemical parameters obtained from the EIS spectra are presented in Table 2. The R_{ct} values are higher for the inhibitor-containing systems than the blank, which implies that the resistance of the steel/electrolyte systems to the charge transfer process is enhanced by the inhibitor molecules. These observations are attributable to the formation of protective film of the inhibitor molecules on the steel surface. The protective film of the inhibitor reduces direct contact of the steel with the aggressive acid solution. All the studied compounds show appreciable values of $\%IE_I$, which are comparable to results obtained from the Tafel polarization measurements. A maximum value of $\%IE_I$ is attained at certain concentration for each compound. Similar observations were recorded from the polarization experiments (*vide supra* section 3.1.1). The lower values of the constant phase element (CPE), Y_0in the presence of the inhibitors compared to the blank indicate that the inhibitor molecules adsorbed on the steel surface to form a protective layer. The values of the CPE exponent, n are close to unity, indicating the pseudo-capacitive characteristics of the electrode/electrolyte systems. The values of n are also indicative of the degree of heterogeneity of the electrode surface. The slightly lower values of n for the inhibited systems compared to the blank suggest that the steel surface is relatively more heterogeneous, which may be due to non-uniform adsorption of the inhibitor molecules on the steel surface.

The magnitudes of the maximum phase angle, $|\theta|$ and slope of the linear portion of the Bode impedance modulus (at intermediate frequencies), $|S|$ are also listed in Table 2. The results show that $|\theta|$ is closer to 90^0, while $|S|$ is closer to 1 at higher concentrations of the inhibitors compared to the blank system. This suggests that the electrode/electrolyte interface behaves closer to an ideal capacitor at higher concentrations of the inhibitors. This also implies that the inhibitor molecules adsorbed on the steel surface to for pseudo-capacitive protective film.

RSC Advances Accepted Manuscript

Table 2. EIS parameters for the corrosion of mild steel in 1 M HCl without and with various concentrations of the inhibitors.

Compound	*Conc.* (ppm)	R_s (Ωcm^2)	R_{ct} (Ωcm^2)	Y_o ($\mu Ss^n cm^{-2}$)	*n*	$\|\theta\|$ (Degree)	$\|S\|$	$\%IE_I$
Blank	-	1.01	28.20	157	0.893	60.59	0.64	-
MS-2-PQPP	5	2.65	42.6	124	0.886	54.68	0.66	34.04
	10	2.67	54.6	124	0.880	57.12	0.70	48.53
	20	1.51	86.8	110.0	0.873	64.52	0.72	67.51
	40	3.64	190	71.9	0.877	64.45	0.78	85.21
	60	2.76	255	61.6	0.869	67.45	0.79	88.98
	80	2.89	337	67.6	0.848	67.08	0.79	91.66
	100	2.93	332	69.9	0.847	67.12	0.79	91.54
MS-3-PQPP	5	3.04	125	78.8	0.878	63.10	0.76	77.52
	10	2.66	259	62.1	0.883	68.90	0.82	89.15
	20	3.18	302	54.2	0.891	69.24	0.83	90.70
	40	3.48	304	58.4	0.868	67.27	0.80	90.76
	60	3.06	431	59.1	0.862	69.38	0.82	93.48
	80	2.99	428	57.1	0.855	68.86	0.81	93.44
	100	2.17	459	57.5	0.867	71.74	0.84	93.88
MS-4-PQPP	5	19.6	134	77.7	0.878	42.60	0.53	79.03
	10	14.6	161	70.3	0.887	49.44	0.61	82.55
	20	17.3	196	63.1	0.879	49.24	0.60	85.66
	40	7.35	255	61.8	0.888	61.75	0.76	88.98
	60	2.14	325	57.5	0.884	71.42	0.84	91.35
	80	2.96	431	68.8	0.863	69.41	0.82	93.48
	100	2.91	436	66.0	0.861	69.86	0.83	93.56
MS-2-PQPMS	5	3.17	178.00	71.98	0.874	65.00	0.77	84.21
	10	2.54	234.00	80.85	0.856	66.83	0.78	87.99
	20	3.48	282.00	66.75	0.854	65.80	0.78	90.04
	40	2.28	365.00	61.56	0.874	70.86	0.83	92.30
	60	2.43	378.00	57.82	0.868	61.08	0.76	92.57
	80	2.33	420.00	60.00	0.854	69.91	0.81	93.30
	100	2.80	384.00	64.90	0.861	69.37	0.82	92.68
MS-3-PQPMS	5	2.26	229.00	63.24	0.876	66.96	0.79	87.73
	10	3.07	247.00	71.63	0.864	52.03	0.64	88.62
	20	2.18	293.00	61.80	0.869	57.24	0.72	90.41
	40	3.20	401.00	54.66	0.875	54.42	0.67	92.99
	60	2.85	395.00	55.67	0.873	70.17	0.83	92.89
	80	2.51	409.00	67.47	0.855	69.67	0.82	93.13
	100	2.52	425.00	64.50	0.857	69.91	0.82	93.39
MS-4-PQPMS	5	2.96	91.39	92.84	0.895	61.79	0.75	69.25
	10	1.98	214.00	67.38	0.869	68.82	0.79	86.87
	20	2.74	256.00	68.93	0.872	67.70	0.80	89.02
	40	2.38	387.00	50.28	0.885	71.81	0.84	92.74
	60	2.59	393.00	56.88	0.872	70.41	0.82	92.85
	80	2.68	398.00	61.72	0.876	70.81	0.83	92.94
	100	2.41	468.00	59.06	0.869	71.39	0.84	94.00

RSC Advances Accepted Manuscript

3.2 Adsorption isotherms

Corrosion inhibition by organic molecules usually results from the adsorption of the inhibitor molecules on the metallic surface. Molecules of inhibitor tend to displace water molecules from the surface of the metal in a reversible process of the form:[45]

$$Inh_{(sol)} + xH_2O_{(ads)} \rightleftharpoons Inh_{(ads)} + xH_2O_{(sol)} \quad (8)$$

where, x is the number of water molecules displaced by one molecule of organic inhibitor (Inh). The adsorption behavior of the studied compounds was investigated by subjecting the experimental data into various adsorption isotherm models including Langmuir, Temkin, and Freundlich isotherms. The data were observed to exhibit the best fits with the Langmuir adsorption isotherm model of the form:[45]

$$\frac{C_{inh}}{\theta} = \frac{1}{K_{ads}} + C_{inh} \quad (9)$$

where C_{inh} is the concentration of the inhibitor, K_{ads} is the equilibrium adsorption constant, and θ is the surface coverage ($\theta = \%IE_I/100$).

Representative isotherm plots are shown in Fig. 4 for MS-2-PQPP and MS-2-PQPMS. The isotherm plots for other compounds (Fig. S4) are also similar. The correlation coefficient (R^2) values of the plots are unity (1.000), while the slopes of the plots are near unity, i.e. 0.98 (MS-2-PQPP), 1.06 (MS-3-PQPP), 1.05 (MS-4-PQPP) 1.07 (MS-2-PQPMS), 1.07 (MS-3-PQPMS), and 1.05 (MS-4-PQPMS). These observations infer the conformity of the data to the linearized Langmuir adsorption isotherm. The values of K_{ads} and ΔG_{ads} are listed in Table 3. The high values of K_{ads} obtained for the studied compounds imply that the displacement of water molecules from the steel surface by the inhibitor molecules, and consequently the adsorption of the inhibitor molecules on the steel surface is a favourable process, and the compounds adsorb strongly on the steel surface. The negative values of ΔG_{ads} also suggest spontaneous adsorption of the inhibitor molecules on the steel surface. It can be inferred from the range of values of ΔG_{ads} in Table 3 that the mode of adsorption of MS-2-PQPP involves competitive physisorption and chemisorption, while the rest of the compounds adsorb mainly via charge sharing (chemisorption). The trend of the values of K_{ads} and ΔG_{ads} is such that MS-3-PQPP > MS-4-PQPP > MS-2-PQPP, and MS-3-PQPMS > MS-2-PQPMS > MS-4-PQPMS, which is the same as the relative order of the *%IE*.

RSC Advances Accepted Manuscript

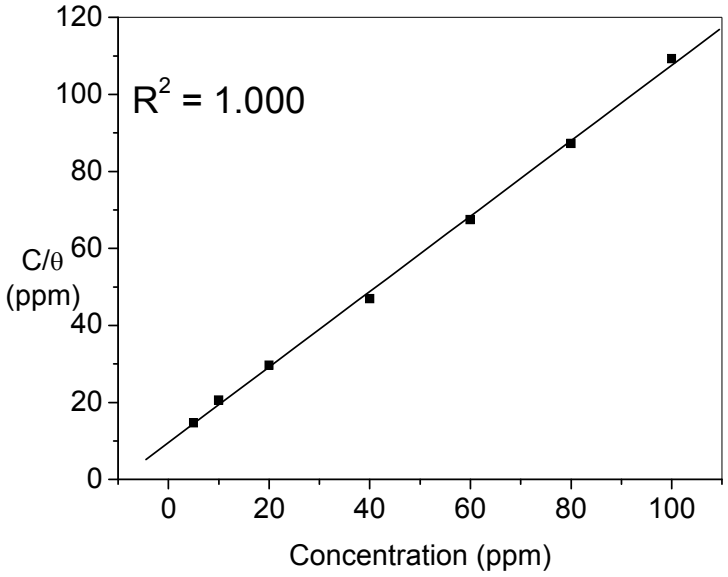

Fig. 4. Langmuir adsorption isotherms for MS-2-PQPP on mild steel in 1 M HCl (*Surface coverage data were taken from the EIS measurements*).

Table 3. Thermodynamic parameters for the adsorption of the studied compounds on mild steel in 1 M HCl at 303.15 K.

Inhibitor	K_{ads} (x10^3)	$-\Delta G_{ads}$ (kJ/mol)
MS-2-PQPP	44.15	37.08
MS-3-PQPP	397.80	42.62
MS-4-PQPP	226.20	41.20
MS-2-PQPMS	692.90	44.02
MS-3-PQPMS	791.10	44.35
MS-4-PQPMS	311.69	42.01

3.3 UV-vis spectroscopic analyses

UV-vis spectroscopic analyses were carried out on the solutions of the studied inhibitor molecules and the resulting solutions after mild steel immersion for 3 hours and the spectra are shown in Fig. 5. The absorption bands at 200 nm – 201 nm in the UV-vis spectra of MS-2-PQPP, MS-3-PQPP and MS-4-PQPP are due to n → π* transition. MS-2-PQPP also shows a shoulder-like band of lower absorbance at 219 nm, while MS-3-PQPPand MS-4-PQPP both show absorption bands at 239 nm and 300 nm – 301 nm due to π → π* transitions and intra-molecular charge transfers (ICT) respectively. MS-2-PQPMS and MS-3-PQPMS show multiple absorption bands at 208 nm – 209 nm, 240 nm, 273 nm, and 327 nm – 329 nm,

RSC Advances Accepted Manuscript

which are due to n→π*, π→π* transitions, and intra-molecular charge transfers (ICT). MS-4-PQPMS shows bands at 206 nm, 242 nm and 285 nm, which can also be attributed to n→π*, π→π* transitions, and intra-molecular charge transfers (ICT) respectively.

After mild steel immersion, MS-2-PQPP shows a new band at 336 nm and the absorbances are generally higher compared to prior mild steel immersion. The major difference in the UV-vis spectra of the solutions of MS-3-PQPP and MS-4-PQPP after mild steel immersion is the increase in absorbance of the bands at 200 nm – 201 nm. MS-2-PQPMS shows additional

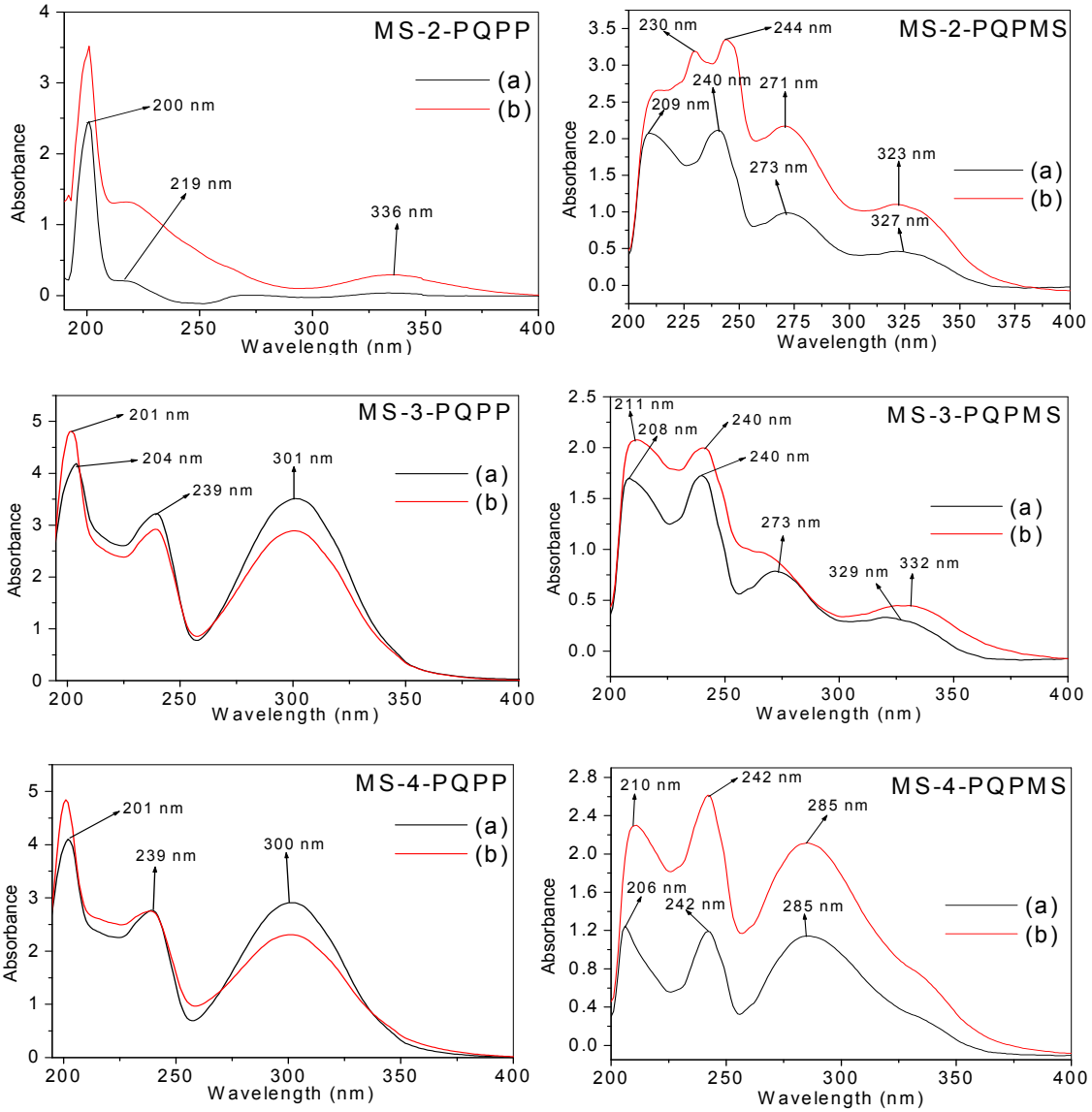

Fig. 5. UV-vis spectra of the acidic solutions of studied inhibitors **(a)** before, and **(b)** after mild steel immersion.

RSC Advances Accepted Manuscript

band at 230 nm, while the band at 240 nm is red-shifted to 244 nm, and those at 273 nm and 327 nm are blue-shifted to 271 nm and 323 nm respectively. For MS-3-PQPMS, the bands at 208 nm and 329 nm shifted to longer wavelengths, appearing at 211 nm and 332 nm respectively, while the one at 273 nm broadens to a shoulder-like band. The band at 206 nm in the UV-vis spectrum of MS-4-PQPMS red-shifted to 210 nm after steel immersion. The changes in the spectra features after mild steel immersion can be attributed to interactions between Fe and the inhibitor molecules and possible formation of Fe-inhibitor complexes.

3.4 Surface morphology

Scanning electron microscopy (SEM) images of mild steel surfaces immersed in 1 M HCl without and with 100 ppm of the studied inhibitors are shown in Fig. 6. The surface of mild steel immersed in 1 M HCl without the inhibitors exhibit highly eroded and damaged features due to unprotected exposure to corrosive ions in the aggressive medium. Mild steel specimens retrieved from the inhibitor-containing solutions show relatively smooth surface. The noticeable roughness on these specimens is mainly due to the polishing scratches introduced to the surface during mechanical abrasion. This again is an indication that the studied compounds adsorb as protective film on mild steel surface and prevent it from direct attack by aggressive ions in the corrosive environment.

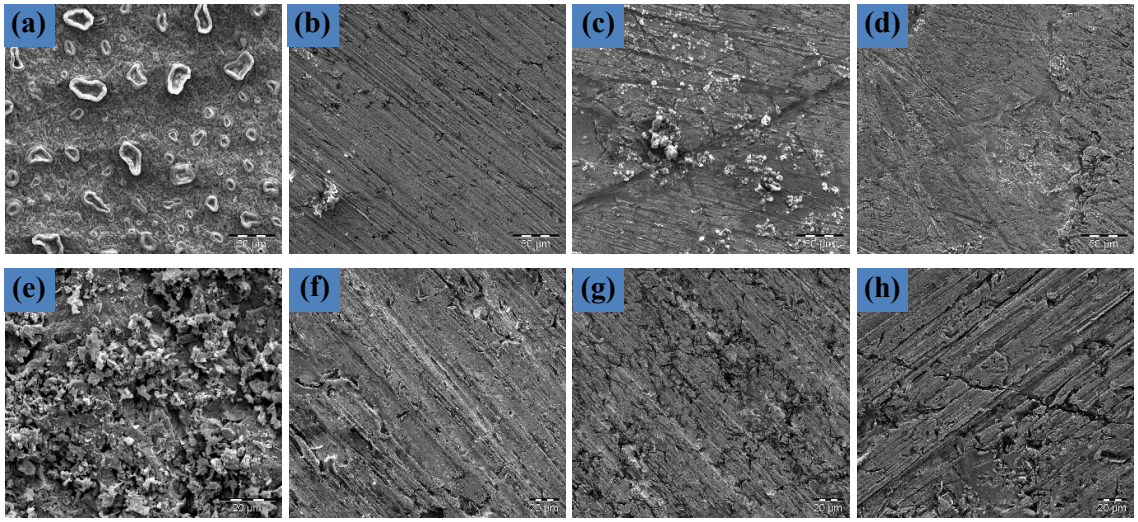

Fig. 6. SEM images of mild steel in 1 M HCl (a & e) without inhibitors, and with 100 ppm of (b) MS-2-PQPP, (c) MS-3-PQPP, (d) MS-4-PQPP, (f) MS-2-PQPMS, (g) MS-3-PQPMS, and (h) MS-4-PQPMS. (*Image size: 50 µm (a-d); 20 µm (e-h)*).

RSC Advances Accepted Manuscript

3.5 Quantum chemical studies

3.5.1 Electron density distributions

The optimized structures the neutral molecules of the studied compounds are shown in Fig. 7, while the corresponding electron density isosurfaces of the HOMO and LUMO are shown in Fig. 8.

The HOMOs of all the molecules comprise both π- and σ- type orbitals, but essentially dominated by π-type molecular orbitals. The HOMO electron density is distributed over the entire pyrazole and phenyl rings. In the MS-n-PQPP series, the N-atom of the methanesulphonamido group (attached to the phenyl ring) and the O-atom of the carbonyl functional group in each case are also involved in the HOMO electron density distributions. In the case of MS-n-PQPMS compounds, the HOMO is extended to the N-atom of the methanesulphonamido group (attached to the phenyl ring) and O-atoms of the methanesulphonamido group (attached to the pyrazole ring). This suggests that the interactions of the studied molecules with mild steel via π-electron donation to the vacant d-orbitals of Fe can occur predominantly around the pyrazole and phenyl rings. The HOMO orbitals around the N-atom of the methanesulphonamido group and the carbonyl O-atom are σ-type, indicating that these groups can interact with vacant p-orbitals of Fe. The S- and O-atoms of the sulphonamido group are not involved in the HOMO electron density distributions.

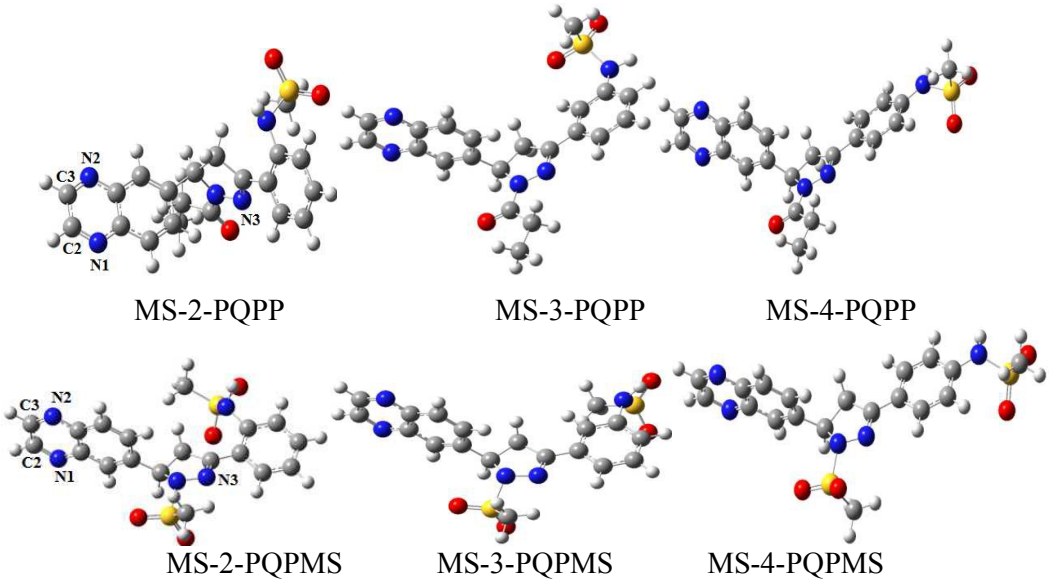

Fig. 7. Optimized structures of the studied compounds (*Selected atomic labels were referred in the discussion of results*).

RSC Advances Accepted Manuscript

The LUMO electron density distributions on the other hand are mainly found on the quinoxaline moieties of the molecules. Apart from the atoms in the quinoxaline ring, the sp^2 N-atom of the pyrazole ring and the C-atoms adjoining the pyrazole and phenyl rings in MS-3-PQPP are also involved in the LUMO electron density surface of the molecule. Some of the C-atoms in the phenyl ring especially those around the sulphonamido groups also contribute to the LUMO electron density distributions in MS-3-PQPP. The LUMO of MS-2-PQPMS is slightly extended to the sp^2 N-atom of the pyrazole ring.The LUMO of MS-3-PQPMS involves the π-electron centre of the C=C group adjoining the pyrazole to the phenyl ring, the sp^2 N-atom of the pyrazole ring, and the C-atom of the phenyl ring adjacent to the methanesulphonamido group.

Fukui indices have been widely used to identify the prospective atomic sites with which an inhibitor molecule interacts with metallic atom.[38,111-114] The atomic sites with highest susceptibility to nucleophilic and electrophilic attacks were predicted by calculating f^+ (for nucleophilic) and f^- (for electrophilic) attacks as:[45]

$$f_k^+ = \rho_{k(N+1)}(r) - \rho_{k(N)}(r) \qquad (10)$$

$$f_k^- = \rho_{k(N)}(r) - \rho_{k(N-1)}(r) \qquad (11)$$

where $\rho_{k(N+1)}$, $\rho_{k(N)}$ and $\rho_{k(N-1)}$ are the electron densities of the k^{th} atom in a specie with N+1, N, and N-1 electrons respectively. The Mulliken population analysis (MPA) and the finite difference (FD) approximations approach introduced by Yang and Mortier[115] was adopted, while the Mulliken gross charges on the atoms were used as the electron densities. Numerical Fukui indices were visualized as graphical isosurfaces with the aid of Multiwfn software[116,117] as shown in Fig. 9.

It is apparent from the f^+ electron density surfaces that for all the inhibitor molecules, the prospective interactions of a negatively charged metallic surface with the inhibitor molecules will occur mainly through the N-atoms and the aromatic centre (C2=C3) in the quinoxaline ring, the sp^2 N-atom (N3) in the pyrazole ring, and the π-electron centre between the C-atoms adjoining the pyrazole and phenyl rings. Some of the C-atoms (in the phenyl ring) especially those in the neighbourhood of the methanesulphonamido group also appear to be prospective sites for nucleophilic attacks. Methanesulphonamido groups are not involved in the f^+ electron density distributions. The most probable sites for electrophilic attacks are depicted with the f^- graphical isosurfaces. In all the inhibitor molecules, the two N-atoms in the pyrazole ring, the carbonyl oxygen, the π-electron centres on the phenyl ring (around the

RSC Advances Accepted Manuscript

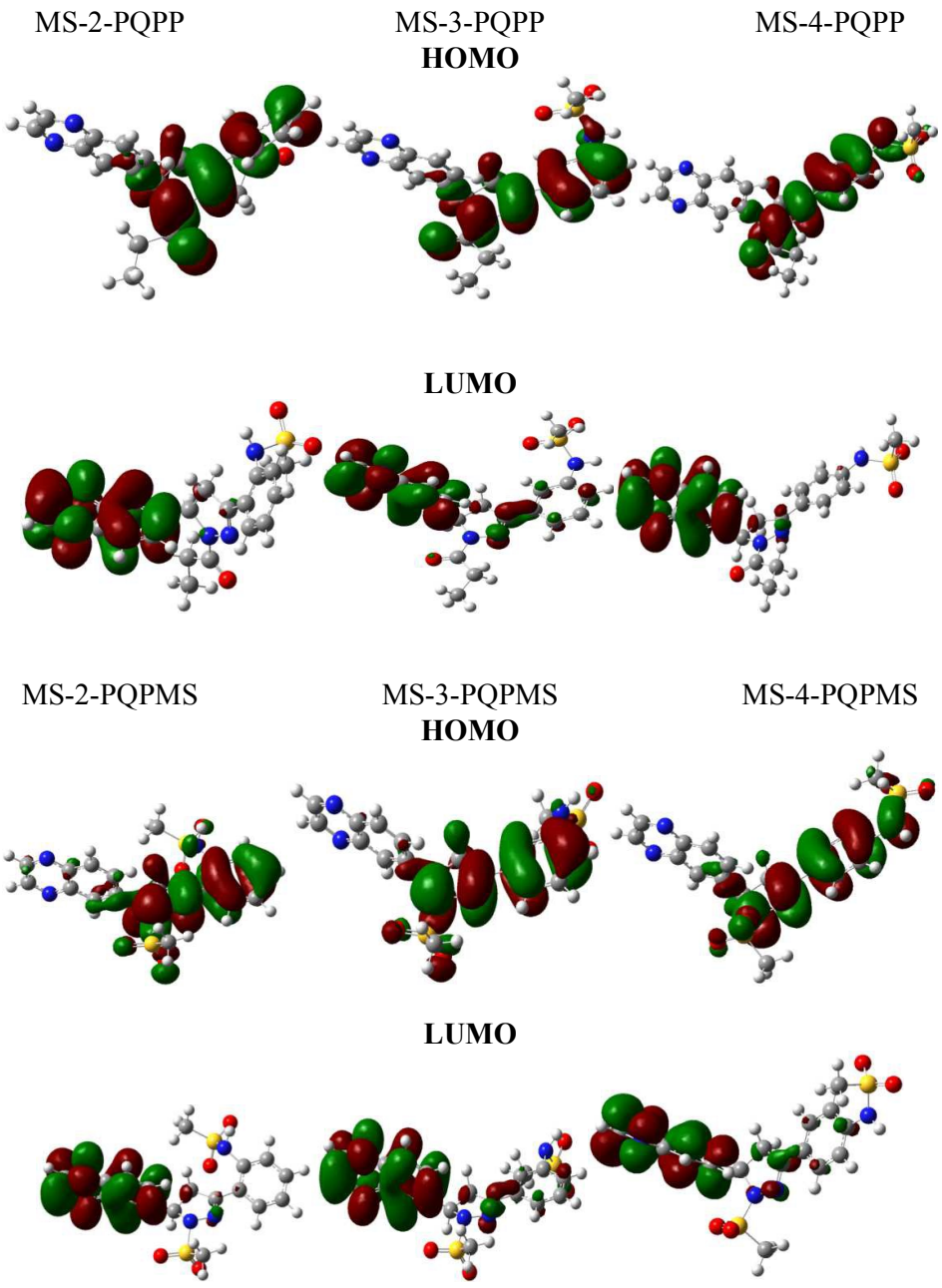

Fig. 8. HOMO and LUMO electron density isosurfaces of the compounds.

point of attachment of the methanesulphonamido group) are prospective sites of electrophilic attacks. These observations suggest that in acidic medium where a positively charged metallic surface overlaid with negatively charged chloride ions (from HCl solution) is present, the studied inhibitors will interact essentially through the quinoxaline ring. On the other hand, positively charged metallic surface or ions can bind to the inhibitor molecules via the pyrazole ring.

RSC Advances Accepted Manuscript

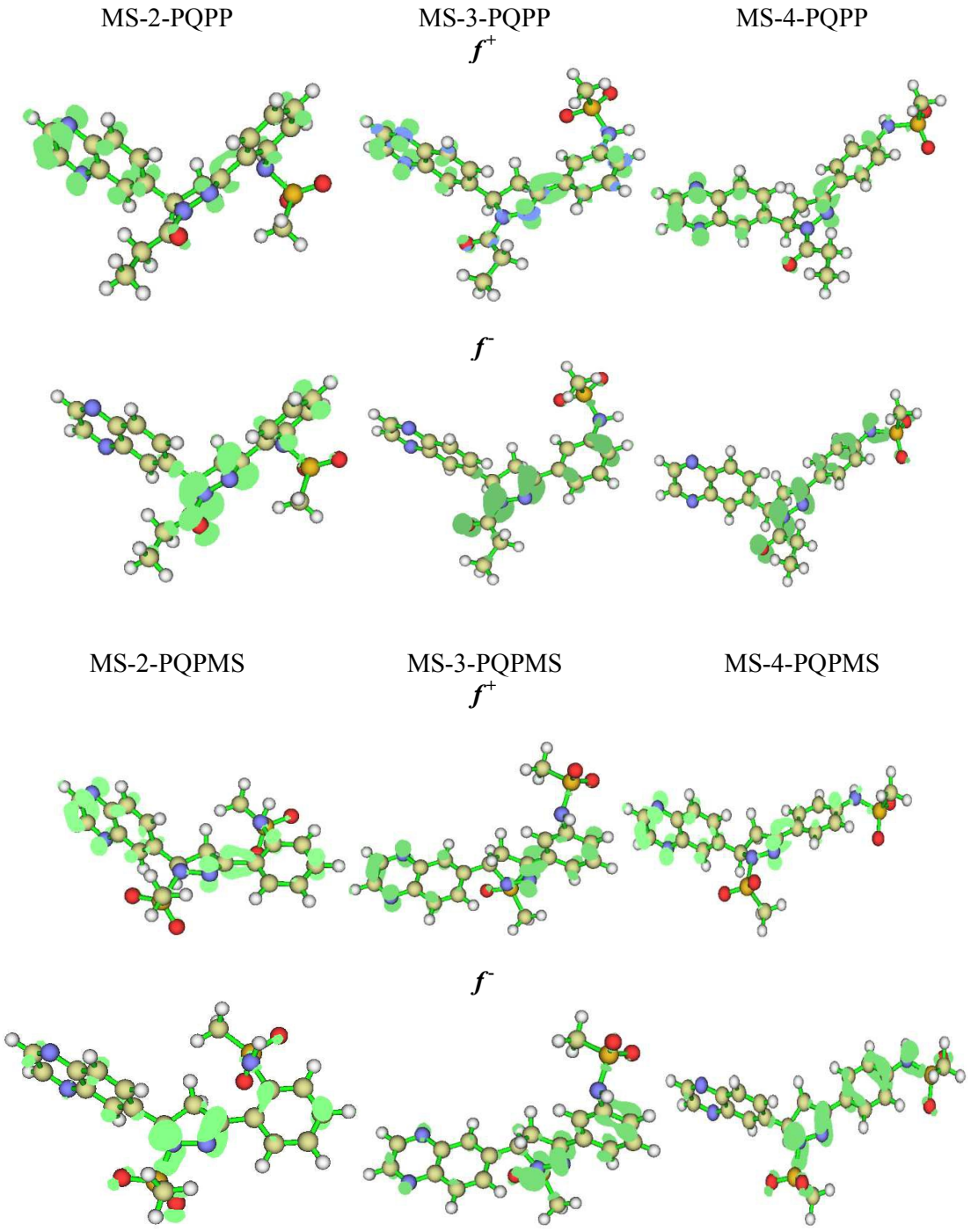

Fig. 9. Fukui functions for the inhibitor molecules (*Isosurface = 0.003*).

3.5.2 Quantum chemical descriptors

Selected quantum chemical parameters for both the neutral and most stable protonated forms of the studied molecules are listed in Table 4. Molecular quantum chemical parameters such as E_{HOMO}, E_{LUMO}, energy gap ($\Delta E_{L-H}=E_{LUMO}-E_{HOMO}$), dipole moment ($\mu$), global

RSC Advances Accepted Manuscript

electronegativity (χ), global hardness (η), and fraction of electrons transferred from an inhibitor to metallic atom (ΔN) are traditionally used to provide molecular based explanation to the relative corrosion inhibition strengths of a set of organic molecules.[9,38,45,47,48,118] Generally, a molecule with higher value of E_{HOMO}, lower value of E_{LUMO} and/or lower value ΔE_{L-H} exhibits higher inhibition efficiency.[6,9,45,48]

In the present study, however, an attempt to correlate individual quantum chemical parameters (Table 4) with average corrosion inhibition efficiencies of the studied molecules could not yield a direct trend. In a case like this, relationships between inhibition efficiencies and quantum chemical parameters are often described by using composite theoretical data. Linear and/or non-linear equations that relate average corrosion inhibition efficiencies with multiple quantum chemical descriptors are obtainable with the aid of quantitative structure

Table 4. Quantum chemical parameters for the neutral and protonated molecules of the inhibitors.

Neutral species						
Parameter	MS-2-PQPP	MS-3-PQPP	MS-4-PQPP	MS-2-PQPMS	MS-3-PQPMS	MS-4-PQPMS
E_{LUMO} *(eV)*	-2.243	-1.942	-1.946	-1.974	-2.051	-1.981
E_{HOMO} *(eV)*	-6.124	-5.983	-5.734	-6.329	-6.444	-6.004
ΔE_{L-H} *(eV)*	3.881	4.041	3.789	4.355	4.393	4.023
χ *(eV)*	4.183	3.963	3.840	4.152	4.248	3.993
η *(eV)*	1.941	2.020	1.894	2.178	2.196	2.012
ΔN	0.726	0.752	0.834	0.654	0.626	0.748
μ *(Debye)*	3.816	5.493	4.505	5.930	3.641	1.049
Protonated species[a]						
Parameters	MS-2-PQPP-$H^+_{(N3)}$	MS-3-PQPP-$H^+_{(O1)}$	MS-4-PQPP-$H^+_{(N2)}$	MS-2-PQPMS-$H^+_{(N3)}$	MS-3-PQPMS-$H^+_{(N1)}$	MS-4-PQPMS-$H^+_{(N1)}$
E_{LUMO} *(eV)*	-6.085	-5.323	-6.962	-6.123	-6.971	-6.971
E_{HOMO} *(eV)*	-9.246	-8.948	-7.947	-9.216	-8.280	-8.041
ΔE_{L-H} *(eV)*	3.160	3.626	0.985	3.093	1.309	1.070
χ *(eV)*	7.665	7.136	7.455	7.670	7.625	7.506
η *(eV)*	1.580	1.813	0.493	1.547	0.654	0.535
ΔN	-0.210	-0.037	-0.462	-0.217	-0.478	-0.473
μ *(Debye)*	4.011	7.772	21.714	6.501	15.592	19.579
PA (kJ/mol)[b]	966.68	938.85	949.61	948.28	945.57	947.57

[a]Data are reported for the most stable protonated species; respective sites of protonation are indicated as subscripts e.g. (N1), (N2) etc. based on atom labeling in Fig. 6, where O1 is the carbonyl oxygen. [b]PA was calculated as previously reported.[45]

activity relationship (QSAR) analysis. QSAR has been successfully used in literature to examine the dependence of average corrosion inhibition strengths of molecules on composite index of more than one quantum chemical descriptors.[47,119,120] Several attempts were made to correlate different linear combinations of relevant parameters with average experimental

RSC Advances Accepted Manuscript

inhibition efficiencies of the molecules. QSAR analyses were performed with the aid of the XLSTAT (Microsoft Excel add-in) software[121] and the results are listed in Table 5.

The results in Table 5 show that composite indices of quantum chemical descriptors including E_{HOMO}, E_{LUMO}, χ, ΔN, μ, and PA correlate well with average inhibition efficiencies of the molecules. The derived QSAR equations were ranked based on nearness of correlation coefficient (R^2) values to unity and small values of the mean square error (MSE) and root-mean-square error (RMSE). When the quantum chemical descriptors for the neutral molecules were used, a linear combination of ΔE_{L-H}, ΔN, μ, and PA gave the best correlation, suggesting that PA plays a role in corrosion inhibition efficiency of the molecules. The best correlation was obtained from a linear combination quantum chemical parameters of the protonated species, that is, ΔE_{L-H}, χ , ΔN, and PA giving R^2 value of 0.998, MSE and RMSE values of 0.546 and 0.739 respectively. The plot of experimental inhibition efficiencies (IE_{exp}) versus predicted inhibition efficiencies (IE_{pred}) (based on the best QSAR equation,

Table 5. Relevant QSAR derived equations and regression analyses data[c].

Parameters	QSAR Equations	R^2	MSE	RMSE
	Neutral species			
E_{HOMO}, E_{LUMO}, ΔN, μ	IE= -553.872 - 97.162*E_{HOMO} +76.955*E_{LUMO} +283.672*ΔN-0.476*μ	0.981	4.705	2.169
ΔE_{L-H}, χ , ΔN, μ	IE = -538.733 + 85.942*ΔE_{L-H} + 18.747*χ +277.212*ΔN – 0.476*μ	0.981	4.719	2.172
ΔE_{L-H}, ΔN, μ, PA	IE = -98.640+58.233*ΔE_{L-H} + 158.817*ΔN-0.415*μ - 0.174*PA	0.990	2.492	1.579
	Protonated species			
ΔE_{L-H}, χ , μ, PA	IE = 708.421+5.056*ΔE_{L-H} + 23.748*χ +0.910*μ-0.866*PA	0.997	0.647	0.805
ΔE_{L-H}, χ , ΔN, PA	IE = 764.510-16.045*ΔE_{L-H} +39.360*χ +110.713*ΔN-0.951*PA	0.998	0.546	0.739
E_{HOMO}, E_{LUMO}, μ, PA	IE = 707.979 - 6.798*E_{LUMO} - 17.033*E_{HOMO} + 0.920*μ - 0.867*PA	0.997	0.649	0.806

[c] $MSE = \sqrt{\sum_{i=1}^{N}\left(IE_{pred} - IE_{exp}\right)^2}$; $RMSE = \sqrt{\frac{1}{n}\sum_{i=1}^{N}\left(IE_{pred} - IE_{exp}\right)^2}$; IE_{pred} = predicted inhibition efficiency; IE_{exp} = experimental efficiency, n is the number of observations (n=6).

IE=764.510-16.045*ΔE_{L-H} +39.360*χ +110.713*ΔN-0.951*PA) is shown in Fig. 10. The results suggest that the corrosion inhibition efficiency of the studied compounds depend on HOMO-LUMO energy gap, electronegativity, fraction of electron transferred to metal, and

RSC Advances Accepted Manuscript

proton affinity, such that lower ΔE_{L-H} and PA, as well as higher χ and ΔN will favour higher protection performance.

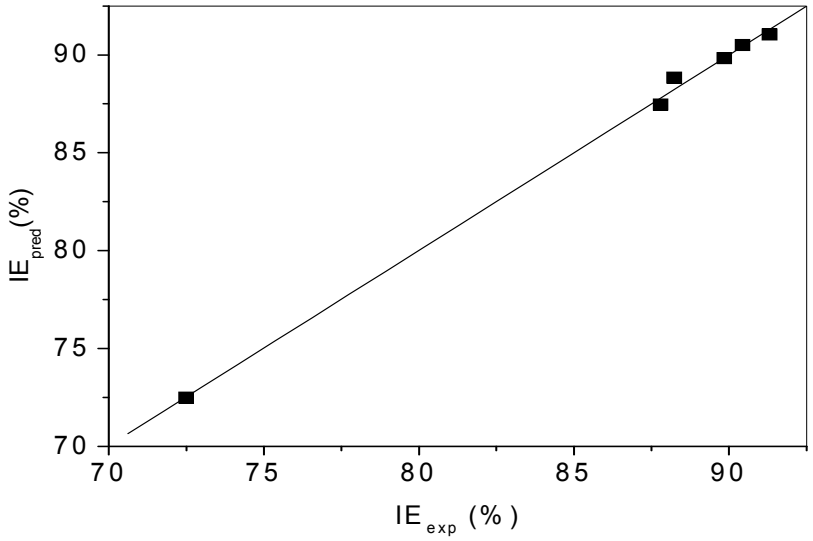

Fig. 10. Plot of observed and predicted IE (%).

3.6 Molecular dynamic (MD) simulations

The lowest energy configurations for the adsorption of the studied inhibitor molecules on Fe(110) surface obtained from MD simulations are shown in Fig. 11. All the inhibitor molecules adopt near-flat orientation on the Fe surface, which supports optimum interactions with metallic substrate. The methyl group of the methanesulphonamido substituent in MS-2-PQPP, MS-2-PQPMS, and MS-4-PQPMS does not adopt parallel inclination with Fe(110) surface. This might minimize the degree of interactions with the metallic surface. This does not happen in the case of MS-3-PQPP and MS-3-PQPMS, which suggests higher degree of interactions between these molecules and Fe(110) substrate.

The interaction and binding energies obtained from the simulations are listed in Table 6. The results show that the order of binding energies of the inhibitor/Fe(110) systems is MS-3-PQPP/Fe(110) > MS-4-PQPP/Fe(110) > MS-2-PQPP/Fe(110), and MS-3-PQPMS/Fe (110) > MS-2-PQPMS/Fe (110) > MS-4-PQPMS/Fe (110) which is in agreement with the trends of observed inhibition strengths of the compounds.

RSC Advances Accepted Manuscript

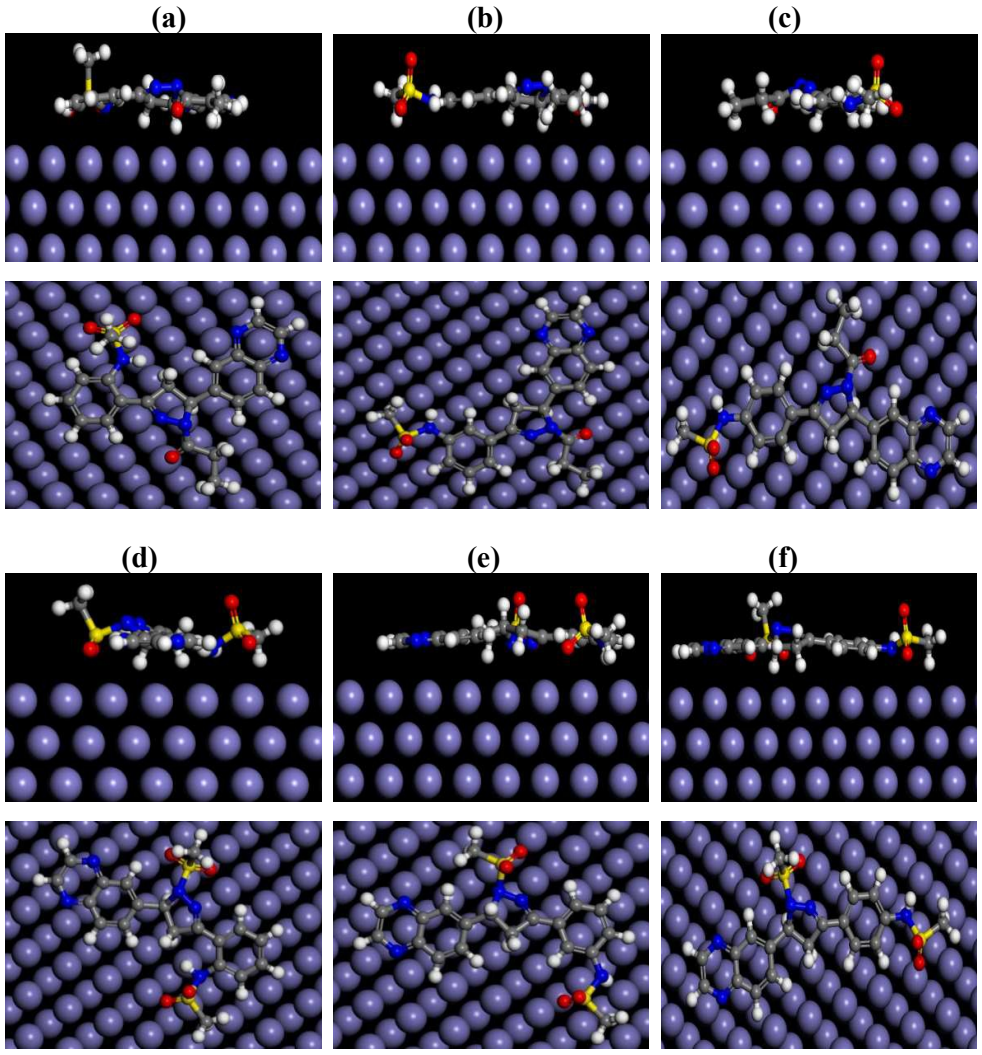

Fig. 11. Side (*above*) and top (*below*) views of the low adsorption energy configurations of (a) MS-2-PQPP, (b) MS-3-PQPP, (c) MS-4-PQPP, (d) MS-2-PQPMS, (e) MS-3-PQPMS, and (f) MS-4-PQPMS interactions with Fe (110) using molecular dynamics simulations.

Table 6. Selected energy parameters for the most stable configurations of the adsorption of the studied inhibitors on Fe (110) surface (in kJ/mol)

System	Interaction energy	Binding energy
Fe (110) + MS-2-PQPP	-976.908	976.908
Fe (110) + MS-3-PQPP	-1113.337	1113.337
Fe (110) + MS-4-PQPP	-1095.693	1095.693
Fe (110) + MS-2-PQPMS	-868.230	868.230
Fe (110) + MS-3-PQPMS	-877.046	877.046
Fe (110) + MS-4-PQPMS	-846.833	846.833

RSC Advances Accepted Manuscript

4 Conclusions

Corrosion inhibition properties of six quinoxalinyl-dihydropyrazolyl-phenyl-methanesulfonamide based compounds were investigated using electrochemical, UV-vis spectroscopy, scanning electron microscopy, quantum chemical calculations, quantitative structure activity relationship, and molecular dynamic simulation studies. The following conclusions can be drawn from the studies:

i. All the studied compounds showed substantial protection performances for mild steel in hydrochloric acid medium. Their inhibition efficiencies increased with increasing concentration up to some limiting values.
ii. All the studied compounds are mixed-type inhibitors; they inhibit both anodic mild steel dissolution and cathodic hydrogen gas evolution and/or oxygen reduction reactions.
iii. The compounds form pseudo-capacitive protective film on mild steel surface and protect the steel from direct acid attack.
iv. The compounds adsorbed on mild steel surface via competitive physisorption and chemisorption mechanisms and their adsorption obeyed the Langmuir adsorption isotherm model.
v. UV-vis spectra suggested inhibitors-Fe interactions, while SEM images confirmed that the compounds protect mild steel surface from direct exposure to corrosive ions.
vi. Quantum chemical descriptors exhibit excellent correlations with inhibition performances and QSAR equations with high correlation coefficients and minimum statistical errors were derived. QSAR analyses suggested the participation of protonated species in the corrosion inhibition process.
vii. Binding energies derived from molecular dynamics simulations are in agreement with the trend of experimental inhibition efficiencies.
viii. Inhibitive strengths were affected by the position of sulfonamido group attached the phenyl ring, such that substitution at position 3 favours higher inhibition potential.

Acknowledgments

L.O.O acknowledges the NRF/Sasol Inzalo foundation for support towards his PhD program. E.E.E acknowledges financial support from NRF (South Africa) for incentive funding for rated researchers. I.B.O is grateful to the Centre of Research Excellence in Corrosion, King Fahd University of Petroleum and Minerals (KFUPM) for support.

RSC Advances Accepted Manuscript

References

1. V. S. Saji, *Recent Pat. Corros. Sci.*, 2010, **2**, 6-12.
2. M. G. Fontana, *Corrosion engineering*, Tata McGraw-Hill Education, 2005.
3. X. Zhang, Y. Zheng, X. Wang, Y. Yan and W. Wu, *Ind. Eng. Chem. Res.*, 2014, **53**, 14199-14207.
4. *Acidizing-Treatment in Oil and Gas Operators*, American Petroleum Institute, DM2014-113, 2014.
5. C. Crowe, J. Masmonteil and R. Thomas, *Oilfield Review*, 1992, **4**, 22-40.
6. P. Singh, E. E. Ebenso, L. O. Olasunkanmi, I. B. Obot and M. A. Quraishi, *J. Phys. Chem. C*, 2016, **120**, 3408-3419.
7. M. E. Mashuga, L. O. Olasunkanmi, A. S. Adekunle, S. Yesudass, M. M. Kabanda and E. E. Ebenso, *Materials*, 2015, **8**, 3607-3632.
8. T. Peme, L. O. Olasunkanmi, I. Bahadur, A. S. Adekunle, M. M. Kabanda and E. E. Ebenso, *Molecules*, 2015, **20**, 16004-16029.
9. L. O. Olasunkanmi, M. M. Kabanda and E. E. Ebenso, *Phys. E*, 2016, **76**, 109-126.
10. D. De la Fuente, I. Díaz, J. Simancas, B. Chico and M. Morcillo, *Corros. Sci.*, 2011, **53**, 604-617.
11. A. Popova, E. Sokolova, S. Raicheva and M. Christov, *Corros. Sci.*, 2003, **45**, 33-58.
12. S. Nesic, J. Postlethwaite and S. Olsen, *Corrosion*, 1996, **52**, 280-294.
13. M. Lagrenee, B. Mernari, M. Bouanis, M. Traisnel and F. Bentiss, *Corros. Sci.*, 2002, **44**, 573-588.
14. M. Nordsveen, S. Nešic, R. Nyborg and A. Stangeland, *Corrosion*, 2003, **59**, 443-456.
15. W.-h. Li, Q. He, S.-t. Zhang, C.-l. Pei and B.-r. Hou, *J. Appl. Electrochem.*, 2008, **38**, 289-295.
16. D. Gandy, *Carbon Steel Handbook*, Electric Power Research Institute *Inc.,* California, USA, 2007.
17. L. C. Murulana, A. K. Singh, S. K. Shukla, M. M. Kabanda and E. E. Ebenso, *Ind. Eng. Chem. Res.*, 2012, **51**, 13282-13299.
18. D. K. Yadav, D. Chauhan, I. Ahamad and M. Quraishi, *RSC Adv.*, 2013, **3**, 632-646.
19. A. A. Al-Amiery, A. A. H. Kadhum, A. B. Mohamad and S. Junaedi, *Materials*, 2013, **6**, 1420-1431.
20. P. B. Raja and M. G. Sethuraman, *Mater. Lett.*, 2008, **62**, 113-116.
21. M. A. Migahed and I. F. Nassar, *Electrochim. Acta*, 2008, **53**, 2877-2882.

RSC Advances Accepted Manuscript

22. E. Bardal, *Corrosion and protection*, Springer Science & Business Media, 2007.
23. G. Gece, *Corros. Sci.*, 2011, **53**, 3873-3898.
24. M. Waring, L. Wakelin and J. Lee, *Biochimica et Biophysica Acta (BBA)-Nucleic Acids and Protein Synthesis*, 1975, **407**, 200-212.
25. T. Zarnowski, Z. Kleinrok, W. Turski and S. Czuczwar, *Neuropharmacology*, 1993, **32**, 895-900.
26. K. I. Priyadarsini, M. F. Dennis, M. A. Naylor, M. R. Stratford and P. Wardman, *J. Am. Chem. Soc.*, 1996, **118**, 5648-5654.
27. H. U. Gali-Muhtasib, M. J. Haddadin, D. N. Rahhal and I. H. Younes, *Oncol. Rep.*, 2001, **8**, 679-684.
28. H. Gao, E. F. Yamasaki, K. K. Chan, L. L. Shen and R. M. Snapka, *Mol. Pharmacol.*, 2003, **63**, 1382-1388.
29. I. Awad, *J. Chem. Technol. Biotechnol.*, 1992, **53**, 227-236.
30. D. Vullo, A. Innocenti, I. Nishimori, J. r. Pastorek, A. Scozzafava, S. Pastoreková and C. T. Supuran, *Bioorg. Med. Chem. Lett.*, 2005, **15**, 963-969.
31. T. J. Welch, W. F. Fricke, P. F. McDermott, D. G. White, M.-L. Rosso, D. A. Rasko, M. K. Mammel, M. Eppinger, M. Rosovitz and D. Wagner, *PloS one*, 2007, **2**, e309.
32. H. Yoshino, N. Ueda, J. Niijima, H. Sugumi, Y. Kotake, N. Koyanagi, K. Yoshimatsu, M. Asada and T. Watanabe, *J. Med. Chem.*, 1992, **35**, 2496-2497.
33. T. A. Msagati and M. M. Nindi, *Talanta*, 2004, **64**, 87-100.
34. C. BAILLY and J. M. WARING, *Biochem. J*, 1998, **330**, 81-87.
35. C. Carisson, M. Johnson and B. Åkerman, *Nucleic Acids Res.*, 1995, **23**, 2413-2420.
36. I. Obot and N. Obi-Egbedi, *Mater. Chem. Phys.*, 2010, **122**, 325-328.
37. I. Obot, N. Obi-Egbedi and N. Odozi, *Corros. Sci.*, 2010, **52**, 923-926.
38. Z. El Adnani, M. Mcharfi, M. Sfaira, M. Benzakour, A. Benjelloun and M. E. Touhami, *Corros. Sci.*, 2013, **68**, 223-230.
39. A. Zarrouk, A. Dafali, B. Hammouti, H. Zarrok, S. Boukhris and M. Zertoubi, *Int. J. Electrochem. Sci*, 2010, **5**, 46-55.
40. I. El Ouali, B. Hammouti, A. Aouniti, Y. Ramli, M. Azougagh, E. Essassi and M. Bouachrine, *J. Mater. Environ. Sci*, 2010, **1**.
41. J. Fu, H. Zang, Y. Wang, S. Li, T. Chen and X. Liu, *Ind. Eng. Chem. Res.*, 2012, **51**, 6377-6386.
42. I. Obot and N. Obi-Egbedi, *Corros. Sci.*, 2010, **52**, 282-285.

RSC Advances Accepted Manuscript

43. M. Elayyachy, B. Hammouti, A. El Idrissi and A. Aouniti, *Port. Electrochim. Acta*, 2011, **29**, 57-68.
44. J. Saranya, P. Sounthari, K. Parameswari and S. Chitra, *Measurement*, 2016, **77**, 175-186.
45. L. O. Olasunkanmi, I. B. Obot, M. M. Kabanda and E. E. Ebenso, *J. Phys. Chem. C*, 2015, **119**, 16004-16019.
46. J. Saranya, P. Sounthari, A. Kiruthuka, K. Parameswari and S. Chitra, *J. Mater. Environ. Sci*, 2015, **6**, 425-444.
47. E. E. Ebenso, T. Arslan, F. Kandemirlı, I. Love, C. l. Öğretır, M. Saracoğlu and S. A. Umoren, *Int. J. Quantum Chem.*, 2010, **110**, 2614-2636.
48. T. Arslan, F. Kandemirli, E. E. Ebenso, I. Love and H. Alemu, *Corros. Sci.*, 2009, **51**, 35-47.
49. A. Samide, B. Tutunaru, C. Negrila and I. Prunaru, *Spectrosc. Lett.*, 2012, **45**, 55-64.
50. L. C. Murulana, M. M. Kabanda and E. E. Ebenso, *RSC Adv.*, 2015, **5**, 28743-28761.
51. S. K. Saha, A. Dutta, P. Ghosh, D. Sukul and P. Banerjee, *Phys. Chem. Chem. Phys.*, 2015, **17**, 5679-5690.
52. N. Soltani, M. Behpour, E. Oguzie, M. Mahluji and M. Ghasemzadeh, *RSC Adv.*, 2015, **5**, 11145-11162.
53. S. A. Umoren, I. B. Obot and Z. M. Gasem, *Ionics*, 2015, **21**, 1171-1186.
54. J. N. Asegbeloyin, P. M. Ejikeme, L. O. Olasunkanmi, A. S. Adekunle and E. E. Ebenso, *Materials*, 2015, **8**, 2918-2934.
55. Y. Sasikumar, A. Adekunle, L. Olasunkanmi, I. Bahadur, R. Baskar, M. Kabanda, I. Obot and E. Ebenso, *J. Mol. Liq.*, 2015, **211**, 105-118.
56. I. Ahamad, R. Prasad and M. Quraishi, *Corros. Sci.*, 2010, **52**, 933-942.
57. K. Ansari, M. Quraishi and A. Singh, *Corros. Sci.*, 2014, **79**, 5-15.
58. H. Elmsellem, T. Harit, A. Aouniti, F. Malek, A. Riahi, A. Chetouani and B. Hammouti, *Prot. Met. Phys. Chem. Surf.*, 2015, **51**, 873-884.
59. A. Ousslim, K. Bekkouch, A. Chetouani, E. Abbaoui, B. Hammouti, A. Aouniti, A. Elidrissi and F. Bentiss, *Res. Chem. Intermed.*, 2014, **40**, 1201-1221.
60. A. Singh, I. Ahamad, V. Singh and M. A. Quraishi, *J. Solid State Electrochem.*, 2011, **15**, 1087-1097.
61. A. K. Singh and M. Quraishi, *Corros. Sci.*, 2011, **53**, 1288-1297.
62. D. K. Yadav, M. Quraishi and B. Maiti, *Corros. Sci.*, 2012, **55**, 254-266.
63. S. A. Ali, M. T. Saeed and S. U. Rahman, *Corros. Sci.*, 2003, **45**, 253-266.

RSC Advances Accepted Manuscript

64. H. Simillion, MSc. Thesis, Vrije Universiteit Brussel, 2012.
65. A. Satapathy, G. Gunasekaran, S. Sahoo, K. Amit and P. Rodrigues, *Corros. Sci.*, 2009, **51**, 2848-2856.
66. R. Patil and S. Radhakrishnan, *Prog. Org. Coat.*, 2006, **57**, 332-336.
67. R. T. Loto, C. A. Loto, A. P. I. Popoola and T. Fedotova, *Arabian J. Chem.*, DOI: http://dx.doi.org/10.1016/j.arabjc.2014.12.024.
68. S. Kharchouf, L. Majidi, M. Bouklah, B. Hammouti, A. Bouyanzer and A. Aouniti, *Arabian J. Chem.*, 2014, **7**, 680-686.
69. S. Umoren and I. Obot, *J. Adhes. Sci. Technol.*, 2014, **28**, 2054-2068.
70. S. Umoren, I. Obot, A. Madhankumar and Z. Gasem, *J. Adhes. Sci. Technol.*, 2015, **29**, 271-295.
71. S. A. Umoren, Z. M. Gasem and I. B. Obot, *Ind. Eng. Chem. Res.*, 2013, **52**, 14855-14865.
72. Z. Tao, S. Zhang, W. Li and B. Hou, *Corros. Sci.*, 2009, **51**, 2588-2595.
73. Y. Abboud, A. Abourriche, T. Saffaj, M. Berrada, M. Charrouf, A. Bennamara, N. Al Himidi and H. Hannache, *Mater. Chem. Phys.*, 2007, **105**, 1-5.
74. X. Li, S. Deng, H. Fu, G. Mu and N. Zhao, *Appl. Surf. Sci.*, 2008, **254**, 5574-5586.
75. A. D. Becke, *J. Chem. Phys.*, 1993, **98**, 5648-5652.
76. R. G. Parr and W. Yang, *J. Am. Chem. Soc.*, 1984, **106**, 4049-4050.
77. C. Lee, W. Yang and R. G. Parr, *Phys. Rev. B*, 1988, **37**, 785.
78. O. h. O. Brovarets, R. O. Zhurakivsky and D. M. Hovorun, *Phys. Chem. Chem. Phys.*, 2014, **16**, 3715-3725.
79. M. Lozynski, D. Rusinska-Roszak and H.-G. Mack, *J. Phys. Chem. A*, 1998, **102**, 2899-2903.
80. S. P. Samijlenko, Y. P. Yurenko, A. V. Stepanyugin and D. M. Hovorun, *J. Phys. Chem. B*, 2010, **114**, 1454-1461.
81. K. B. Wiberg, *J. Comput. Chem.*, 2004, **25**, 1342-1346.
82. M. J. Frisch, G. W. Trucks, H. B. Schlegel, G. E. Scuseria, M. A. Robb, J. R. Cheeseman, G. Scalmani, V. Barone, B. Mennucci and G. A. Petersson, et al., Gaussian 09 (Revision D.01), Gaussian, Inc., Wallingford, CT, 2009.
83. F. Jensen, *Introduction to Computational Chemistry*, John Wiley & Sons Ltd., England, 2nd edn., 2007.
84. L. H. Mendoza-Huizar and C. H. Rios-Reyes, *J. Mex. Chem. Soc.* 2011, **3**, 142-147.
85. S. Martinez, *Mater. Chem. Phys.*, 2003, **77**, 97-102.

RSC Advances Accepted Manuscript

86. R. G. Pearson, *Inorg. Chem.*, 1988, **27**, 734-740.
87. A. B. Anderson and S. Mehandru, *Surf. Sci.*, 1984, **136**, 398-418.
88. K. Khaled, *J. Solid State Electrochem.*, 2009, **13**, 1743-1756.
89. A. Arya and E. A. Carter, *J. Chem. Phys.*, 2003, **118**, 8982-8996.
90. A. Arya and E. A. Carter, *Surf. Sci.*, 2004, **560**, 103-120.
91. L. Guo, X. Ren, Y. Zhou, S. Xu, Y. Gong and S. Zhang, *Arabian J. Chem.*, 2015.
92. X. Luo, S. Zhang and L. Guo, *Int. J. Electrochem. Sci*, 2014, **9**, 7309-7324.
93. A. Singh, Y. Lin, M. A. Quraishi, L. O. Olasunkanmi, O. E. Fayemi, Y. Sasikumar, B. Ramaganthan, I. Bahadur, I. B. Obot and A. S. Adekunle, *Molecules*, 2015, **20**, 15122-15146.
94. J. Tan, L. Guo, T. Lv and S. Zhang, *Int. J. Electrochem. Sci*, 2015, **10**, 823-837.
95. S. W. Bunte and H. Sun, *J. Phys. Chem. B*, 2000, **104**, 2477-2489.
96. G. Liu, S. Chen, M. Hongfang and X. Liu, *J. Serbian Chem. Soc.*, 2007, **72**, 475-484.
97. M. J. McQuaid, H. Sun and D. Rigby, *J. Comput. Chem.*, 2004, **25**, 61-71.
98. H. Sun, P. Ren and J. Fried, *Comput. Theor. Polym. Sci.*1998, **8**, 229-246.
99. J. Yang, Y. Ren, A.-m. Tian and H. Sun, *J. Phys. Chem. B*, 2000, **104**, 4951-4957.
100. A. Fouda, A. Al-Sarawy and E. El-Katori, *Desalination*, 2006, **201**, 1-13.
101. M. Morad and A. K. El-Dean, *Corros. Sci.*, 2006, **48**, 3398-3412.
102. Y. Yan, W. Li, L. Cai and B. Hou, *Electrochim. Acta*, 2008, **53**, 5953-5960.
103. E. E. Stanbury and R. A. Buchanan, *Fundamentals of Electrochemical Corrosion*, ASM International, Materials Park, Ohio, USA. Pg. 3-6.
104. P. Cao, R. Gu and Z. Tian, *Langmuir*, 2002, **18**, 7609-7615.
105. C. Cao, *corrosion science*, 1996, **38**, 2073-2082.
106. I. Lozano, E. Mazario, C. Olivares-Xometl, N. Likhanova and P. Herrasti, *Materials Chemistry and Physics*, 2014, **147**, 191-197.
107. F. S. de Souza and A. Spinelli, *Corros. Sci.*, 2009, **51**, 642-649.
108. S. A. Umoren, Y. Li and F. H. Wang, *Corros. Sci.*, 2010, **52**, 1777-1786.
109. A. A. Al-Amiery, A. A. H. Kadhum, A. B. Mohamad, A. Y. Musa and C. J. Li, *Materials*, 2013, **6**, 5466-5477.
110. H. Cang, Z. Fei, W. Shi and Q. Xu, *Int. J. Electrochem. Sci*, 2012, **7**, 10121-10131.
111. L. Larabi, O. Benali, S. Mekelleche and Y. Harek, *Appl. Surf. Sci.*, 2006, **253**, 1371-1378.
112. J. Cruz, R. Martınez, J. Genesca and E. Garcıa-Ochoa, *J. Electroanal. Chem.*, 2004, **566**, 111-121.

RSC Advances Accepted Manuscript

113. G. Gece, *Corros. Sci.*, 2008, **50**, 2981-2992.
114. L. M. Rodríguez-Valdez, W. Villamisar, M. Casales, J. Gonzalez-Rodriguez, A. Martínez-Villafañe, L. Martinez and D. Glossman-Mitnik, *Corros. Sci.*, 2006, **48**, 4053-4064.
115. W. Yang and W. J. Mortier, *J. Am. Chem. Soc.*, 1986, **108**, 5708-5711.
116. T. Lu and F. Chen, *J. Comput. Chem.*, 2012, **33**, 580-592.
117. T. Lu and F. Chen, *J. Mol. Graphics Modell.*, 2012, **38**, 314-323.
118. S. T. Arab, *Mater. Res. Bull.*, 2008, **43**, 510-521.
119. K. Khaled, *Appl. Surf. Sci.*, 2006, **252**, 4120-4128.
120. K. Khaled, K. Babić-Samardžija and N. Hackerman, *Electrochim. Acta*, 2005, **50**, 2515-2520.
121. Addinsoft, XLSTAT (2016.02), http://www.xlstat.com, 2016.

RSC Advances Accepted Manuscript

Table of Content Entry

The experimental corrosion inhibition properties were supported by detailed theoretical studies that revealed dependence of protection efficiency on proton affinity.

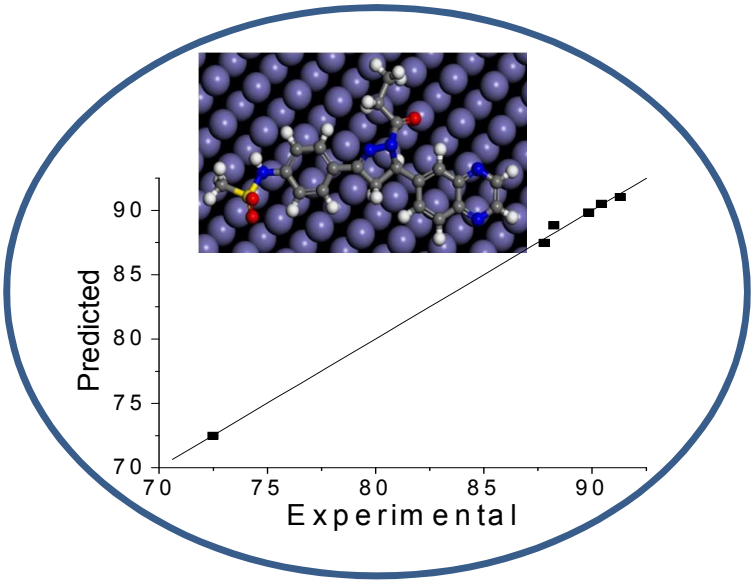

RSC Advances Accepted Manuscript